JOURNAL OF SYNCHROTRON RADIATION
ISSN 1600-5775

Collimating Montel mirror as part of a multi-crystal analyzer system for resonant inelastic X-ray scattering

Jungho Kim,* Xianbo Shi, Diego Casa, Jun Qian, XianRong Huang and Thomas Gog

Advanced Photon Source, Argonne National Laboratory, 9700 South Cass Avenue, Argonne, IL 60439, USA.
*Correspondence e-mail: jhkim@aps.anl.gov

Received 26 January 2016
Accepted 4 May 2016

Edited by G. E. Ice, Oak Ridge National Laboratory, USA

Keywords: X-ray optics; multilayer mirror; X-ray collimation; resonant inelastic X-ray scattering.

Advances in resonant inelastic X-ray scattering (RIXS) have come in lockstep with improvements in energy resolution. Currently, the best energy resolution at the Ir L_3-edge stands at ∼25 meV, which is achieved using a diced Si(844) spherical crystal analyzer. However, spherical analyzers are limited by their intrinsic reflection width. A novel analyzer system using multiple flat crystals provides a promising way to overcome this limitation. For the present design, an energy resolution at or below 10 meV was selected. Recognizing that the angular acceptance of flat crystals is severely limited, a collimating element is essential to achieve the necessary solid-angle acceptance. For this purpose, a laterally graded, parabolic, multilayer Montel mirror was designed for use at the Ir L_3-absorption edge. It provides an acceptance larger than 10 mrad, collimating the reflected X-ray beam to smaller than 100 µrad, in both vertical and horizontal directions. The performance of this mirror was studied at beamline 27-ID at the Advanced Photon Source. X-rays from a diamond (111) monochromator illuminated a scattering source of diameter 5 µm, generating an incident beam on the mirror with a well determined divergence of 40 mrad. A flat Si(111) crystal after the mirror served as the divergence analyzer. From X-ray measurements, ray-tracing simulations and optical metrology results, it was established that the Montel mirror satisfied the specifications of angular acceptance and collimation quality necessary for a high-resolution RIXS multi-crystal analyzer system.

1. Introduction

Since the pioneering study of NiO (Kao *et al.*, 1996), hard X-ray resonant inelastic X-ray scattering (RIXS) has made remarkable progress as a spectroscopic technique at synchrotron radiation facilities such as the Advanced Photon Source (APS). The unique capability of RIXS to provide element-specific excitation spectra in complex materials by measuring their momentum- and energy-dependences has brought it to the forefront of experimental photon science (Ament *et al.*, 2011). These advances have come in lockstep with improvements in energy resolution of RIXS spectrometers, which typically are based on diced spherical crystal analyzers. For the case of the Ir L_3-edge using a Si(844) reflection, the best resolution achieved to date is ∼25 meV (Gog *et al.*, 2013).

Recently, iridium oxides have been the subject of intense study. The strong relativistic spin-orbit coupling in these compounds provides a fascinating mix of novel electronic and magnetic phases and quantum phenomena (Jackeli & Khaliullin, 2009; Kim *et al.*, 2008, 2009). RIXS studies have demonstrated that high-resolution spectra yield important information on the spin and orbital dynamics that could not

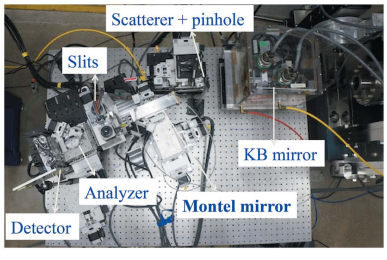

have been gained otherwise (Kim *et al.*, 2012*a*,*b*, 2014). Yet some of these compounds have remained inaccessible due to the inherently small energy scales of intriguing phenomena that cannot be resolved with the current energy resolution. The resonant character of RIXS limits the selection of available near-backscattering analyzer reflections at the corresponding absorption edge. For the few reflections that are suitable, the energy resolution is determined by their intrinsic symmetric reflection width, which cannot be reduced. One way to circumvent this limitation and achieve better resolution is to employ an assembly of multiple, flat, asymmetric crystals, as has been proposed (Huang, 2011).

However, a practical RIXS instrument requires a rather large solid-angle acceptance in order to collect sufficient scattered photons from the sample. Compared with spherical analyzers, the acceptance of flat crystal optics is typically orders of magnitude smaller, making it imperative to introduce a collimating optical element that can collect scattered X-rays with sufficiently large acceptance, while delivering well collimated X-rays to the multi-crystal analyzer system, thus achieving the desired energy resolution at practical count rates. For this purpose, a laterally graded, parabolic, multilayer Montel mirror was chosen, where two one-dimensionally figured multilayer mirrors are joined orthogonally along their edges. This design was chosen for its superior surface figuring, compact design, ease of alignment and mechanical stability, when compared with more traditional designs such as a Kirkpatrick–Baez (KB) configuration (Honnicke *et al.*, 2011). Similar analyzer systems have been designed and implemented at the APS and the National Synchrotron Light Source II for 9 keV photon energy (Honnicke *et al.*, 2011; Cai *et al.*, 2013; Shvyd'ko *et al.*, 2014; Mundboth *et al.*, 2014; Suvorov *et al.*, 2014).

Previous studies on Montel mirrors typically determined the collimation performance indirectly by measuring the focusing performance and simulating the collimation (Honnicke *et al.*, 2011; Mundboth *et al.*, 2014). In the present work, detailed collimating characteristics were measured directly at beamline 27-ID at the Advanced Photon Source. X-rays from a diamond (111) monochromator illuminated a scattering source of diameter 5 µm, generating an incident beam on the mirror with a well determined divergence of 40 mrad. A flat Si(111) crystal after the mirror in combination with a position-sensitive detector served as the divergence analyzer. Based on X-ray measurements, ray-tracing simulations, optical metrology results and employing a realistic scattering source, the collimation performance of the mirror is evaluated and its suitability as the collimator of a multi-crystal analyzer system is assessed.

2. Design parameters of the Montel mirror

The Montel mirror consists of two separate, laterally graded, parabolic multilayer mirrors, joined orthogonally in an L-shape configuration along their edge. The lateral grading in the period of the multilayer is required to maintain high reflectivity for varying incident angles along its length. The mirror is intended to collimate scattered X-rays from a point source in the vicinity of the Ir L_3-absorption edge ($\sim$11.215 keV) in both vertical and horizontal directions. The angular acceptance and divergence of the reflected beam for both mirror surfaces were designed to be >10 mrad and <100 µrad, respectively. Manufacturing specifications such as parabolic shape, overall dimensions, choices of multilayer reflector and spacer elements were selected to be consistent with requirements of a multi-crystal analyzer system, which are working distance, solid-angle coverage, collimation quality and, ultimately, the capability of achieving <10 meV energy resolution at the Ir L_3-edge when using a scattering source of a few micrometers in size. The collimation quality targeted requires tight manufacturing tolerances for shape- and slope-errors, multilayer width- and grading-errors, interlayer-roughness and diffusion. The design parameters of the Montel mirror are summarized in Table 1. Fig. 1(*a*) shows the quadratic function describing the designed lateral multilayer spacing profile. Using such a profile, the calculated reflectivity remains above 80% for almost the entire length of the mirror, as shown by the red curve in Fig. 1(*b*), making the benefit of grading evident. For comparison, the calculated reflectivity of a non-graded multilayer mirror with constant spacing of 32 Å is also shown in Fig. 1(*b*) (black curve). In this case, a high reflectivity can only be achieved at the center of the mirror.

Table 1
Design parameters of the Montel mirror.

Wavelength / energy	0.1106 nm / 11215 eV
Multilayer reflector / spacer	Ruthenium / carbon
Multilayer spacing at center, Λ_0	32 Å
Gamma ratio	0.4
Interlayer roughness	$\leq$3 Å r.m.s.
Number of layers	120
Dimensions	150 mm × 7 mm × 7 mm
Angular acceptance angles	>10 mrad in both directions
Expected reflectivity	>80% for a single mirror
Bragg angle at center, θ_B	1.02° (17.8 mrad)
Substrate	Si (100)
Vertex radius (parabolic parameter p†)	0.127 mm
Source-to-mirror distance (D_{SM})	200 mm

† The parabolic parameter p is from the equation $y^2 = 2px$.

The Montel mirror was manufactured by Incoatec GmbH. The manufacturer's own characterization, which is not included in this paper, confirmed that the multilayer spacing values are within the specified tolerance of ±1.0% along the entire length of both surfaces.

3. Measurement setup

The measurement setup at beamline 27-ID is shown in Fig. 2. A high-heat-load diamond (111) double-crystal monochromator provided an incident photon beam at 11.215 keV, which was focused onto a plexiglass scatterer by a set of KB mirrors. A 5 µm pinhole was placed at a distance of 3 mm and an angle of 20°, which together with the plexiglass creates a scattering source with a well defined divergence. The pinhole also functions as an incident beam stop. Focusing the incident beam with the KB mirrors increases the number of scattered

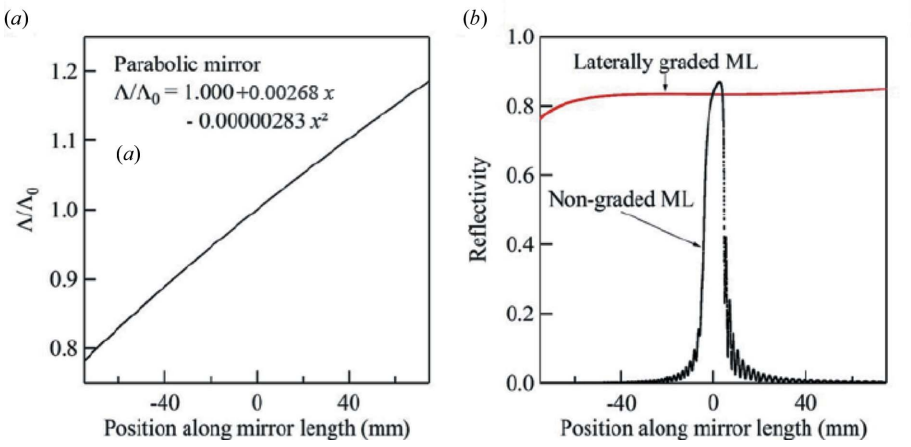

Figure 1
(*a*) Profile of the lateral multilayer spacing (Λ) along the length of the mirror, with respect to the spacing Λ_0 at the center. (*b*) Calculated reflectivity of a laterally graded multilayer (red), with a non-graded multilayer for comparison (black).

photons through the pinhole. The focus was adjusted to set a divergence of ∼40 mrad, as estimated by measuring the effective size of the scattering source as seen through the pinhole. The Montel mirror was initially positioned at the nominal working distance and angle in such a way to allow separate measurements of reflected beams in vertical, horizontal and combined directions. The Montel mirror was fitted by the manufacturer with fixed entrance and exit apertures with sizes of 1.9 mm × 1.9 mm and 2.8 mm × 2.8 mm, respectively. In order to minimize the scattering background, additional slits were placed after the Montel mirror. A one-dimensional (1D) position-sensitive detector with a resolution of 50 µm was used to align the Montel mirror and measure the spatial profiles of reflected beams. In combination with a flat Si(111) crystal, this detector is also used to measure the beam divergence.

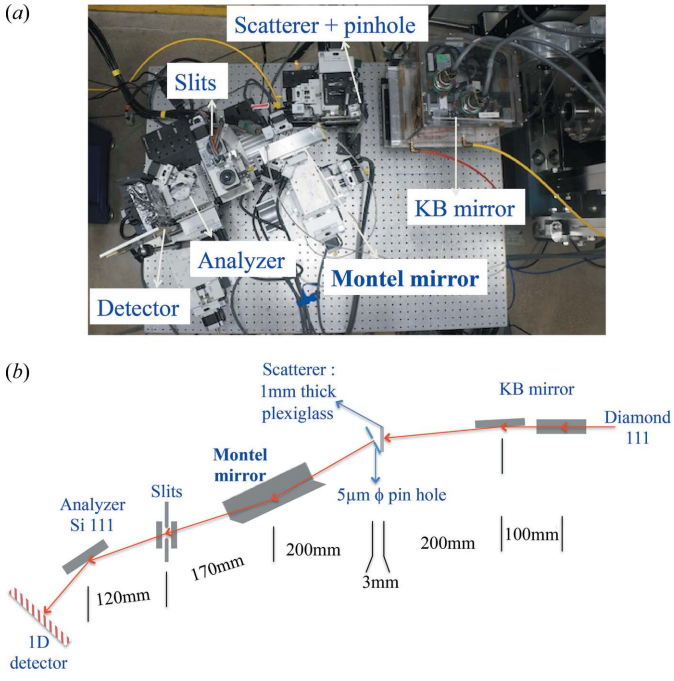

Figure 2
Experimental setup shown in a photograph (*a*) and in a schematic diagram (*b*). A 5 µm pinhole together with a plexiglass plate create a scattering source with a well defined divergence. The 1D position-sensitive detector and the Si (111) crystal are used to measure spatial beam profiles and beam divergence.

4. Experimental results

4.1. Metrology measurement

In order to achieve the required collimation performance, it is critical that slope errors of the Montel mirror are kept to a minimum. Figs. 3(*a*) and 3(*b*) show optical line profiles along the centerline of each mirror surface, as measured at the APS with a long trace profiler. The two orthogonal mirror surfaces are denoted as mirror surface 1 (MS1) and mirror surface 2 (MS2). The midpoint of each centerline is indicated by $x = 0$, with $x < 0$ and $x > 0$ corresponding to the near and far end of the mirror relative to the scattering source. The height error profiles were obtained by subtracting the ideal parabolic curve for $p = 0.127$ mm from the measured height profiles. Standard

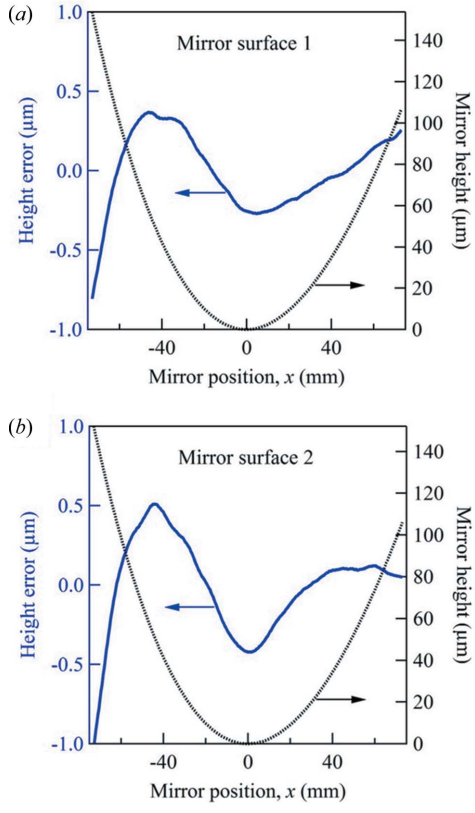

Figure 3
Height profiles and height errors for (*a*) MS1 and (*b*) MS2, as obtained by subtracting the ideal parabolic curve for $p = 0.127$ mm from the measured height profiles.

deviations of the height- and slope-errors were found to be 237 nm and 24 µrad for MS1, and 293 nm and 32 µrad for MS2. As shown in Figs. 3(*a*) and 3(*b*), for both mirror surfaces these figure errors are significant for $x < 0$, and become even more severe at $x < -40$ mm.

4.2. Alignment and optimization of the Montel mirror

Figs. 4(*a*) and 4(*b*) illustrate the separation of the four emerging beams from the Montel mirror; the direct beam, two singly and one doubly reflected beam. The singly reflected beams are separately deflected by either MS1 or MS2 and appear at a vertically or horizontally shifted position from the direct beam, while the doubly reflected beam is sequentially deflected by both surfaces and is shifted from the direct beam in both horizontal and vertical directions, as shown in Fig. 4(*b*). The doubly reflected beam is collimated in both directions and constitutes the sought-after output from this device.

For coarse alignment of the Montel mirror a 28 mm × 28 mm Si-PIN detector was used, large enough to potentially capture all four beams. With the slit fully open, the incident angle of MS1 was first scanned. A sharp peak was observed near $\theta_B = 1.02°$, consistent with expectations. Then, the vertical slit was set to block the direct beam. Subsequently, the angle of MS2 was adjusted. Again, a sharp peak was observed near $\theta_B = 1.02°$, corresponding to the doubly reflected beam. The horizontal slit was then set to allow only the doubly reflected beam to pass.

Fine alignment consisted of optimizing the distance D_{SM} between the scattering source and the Montel mirror, which is crucial to obtain the designed collimation performance. For this purpose, a flat Si(111) crystal in combination with a position-sensitive detector, serving as the divergence analyzer, was placed after the slit (*cf.* Fig. 2). D_{SM} was optimized by finding the smallest full width at half-maximum (FWHM) of the analyzer rocking curve. The resulting distance was 197 mm, close to the design value of 200 mm.

4.3. Reflected beam profile

Figs. 4(*c*) and 4(*d*) show spatial profiles of all reflected beams after alignment. The 1D detector was placed at about 230 mm from the center of the Montel mirror with no slits and analyzer crystal present. The top scales in Figs. 4(*c*) and 4(*d*) indicate the position of reflected beams on the detector. The doubly reflected beam is separated from the singly reflected beam by ∼8.2 mm, which agrees with the calculated value, $2 \times \theta_B \times 230$ mm = 8.2 mm. The bottom scales under the doubly reflected beam indicate the position along the mirror length, x.

From the widths of the doubly reflected beam in each of the spatial profiles the effective optical length and the corresponding effective angular acceptance can be determined. The design length of the mirror of 150 mm at a working distance of 197 mm corresponds to a nominal angular acceptance of 15.8 mrad and a collimated beam width of 2.7 mm at the 1D detector. For MS1, as shown in Fig. 4(*c*), the measured width (top axis) is ∼2.0 mm, corresponding to an effective optical length of ∼111 mm and an angular acceptance of ∼11 mrad. For MS2, the measured full width is ∼2.5 mm corresponding to an effective optical length of ∼139 mm and an angular acceptance of ∼14 mrad. However, if the low-intensity shoulder on the left side is excluded, the width is reduced to ∼2.2 mm, corresponding to an effective optical length of ∼122 mm and an angular acceptance of ∼12 mrad. For both mirrors, the near ends ($x < -40$) seem to reflect the beam rather poorly, probably due to the large figure error near that end (*cf.* Fig. 3). Also, misaligned fixed entrance- and exit-apertures could be a contributing factor.

Regarding mirror reflectivity, a preliminary measurement at the mirror center showed a reflectivity of ∼80%, consistent with expectation. A full reflectivity profile was not recorded at this point.

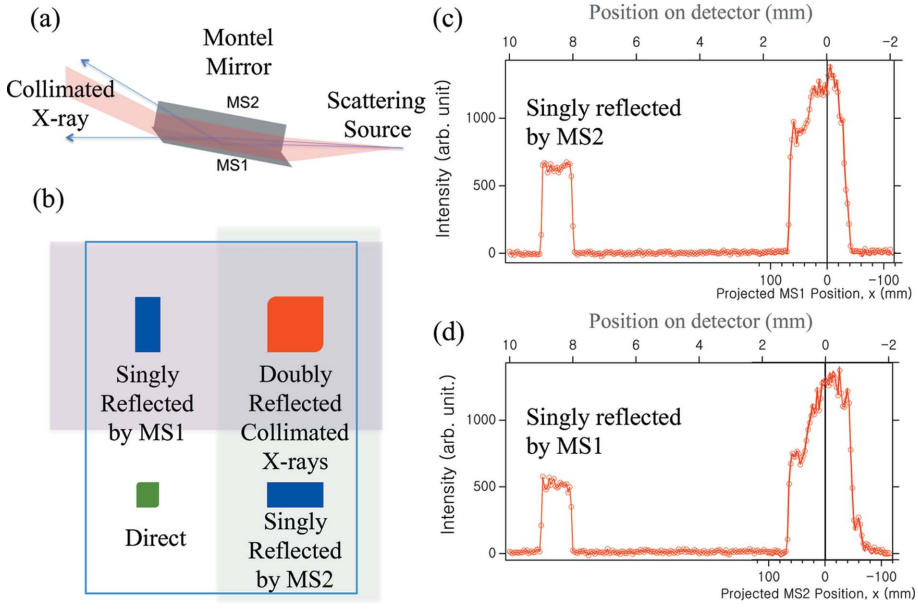

Figure 4
(*a*) Montel mirror reflection geometry. (*b*) Schematic of exit beams downstream of the Montel mirror. (*c*) and (*d*) Measured spatial profiles of reflected beams in horizontal and vertical directions, respectively.

4.4. X-ray angular divergence measurements

Measurements of the divergence of the collimated exit beam were accomplished using a flat Si (111) crystal after the mirror in combination with the 1D detector. The incident bandpass from the diamond (111) monochromator together with the intrinsic width of the symmetric Si (111) reflection results in a calculated rocking-curve width of

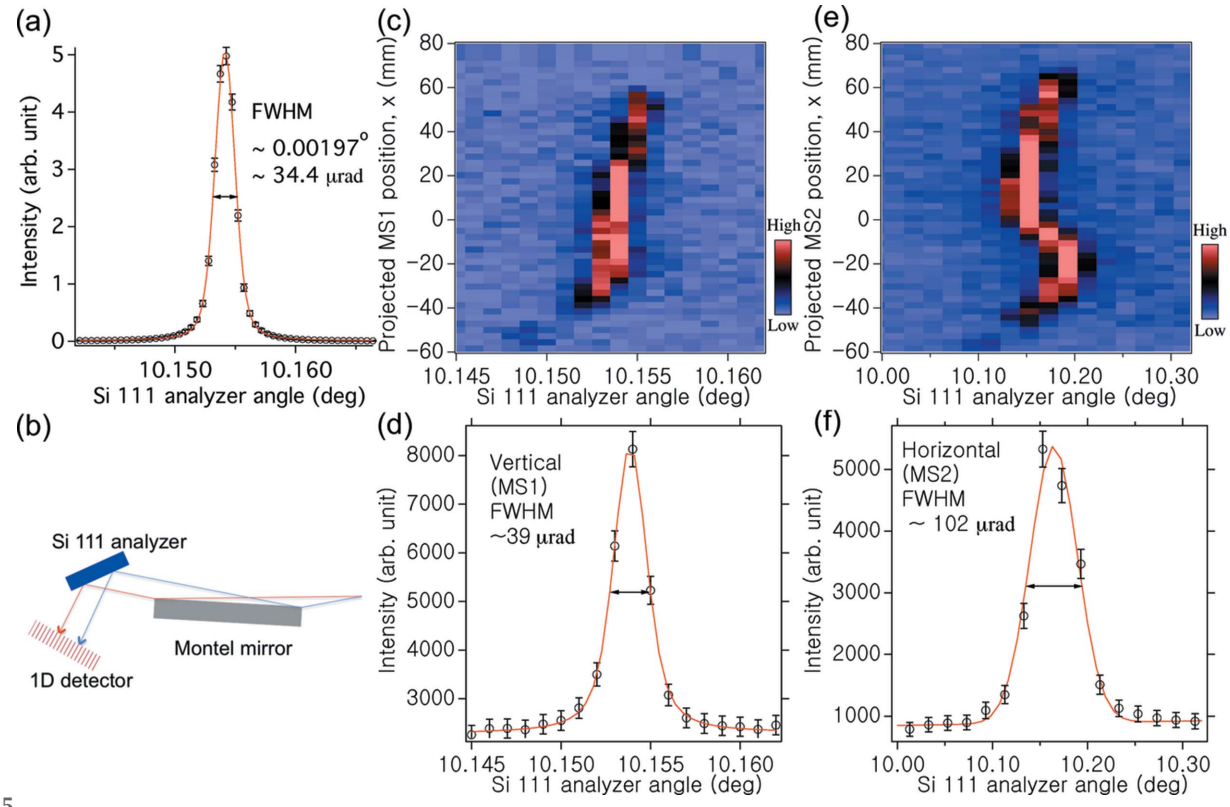

Figure 5
(*a*) Measured rocking curve of the Si(111) divergence analyzer without the mirror. (*b*) Schematic diagram of the angular divergence measurement. (*c*) and (*e*) 2D plots of divergence measurements (horizontal axis) *versus* position along the mirror (vertical axis) for MS1 and MS2, respectively. (*d*) and (*f*) Integrated rocking curves for MS1 and MS2, respectively.

34.6 μrad. Fig. 5(*a*) shows the measured rocking curve of the divergence analyzer without the mirror. A Voigt fit yields a FWHM of 34.4 μrad, consistent with the calculated value. A schematic diagram of the angular divergence measurement in one direction is shown in Fig. 5(*b*). The collimated rays from different positions on the mirror surface are mapped onto different positions on the 1D detector, thus the divergence of exit rays originating at different points on the mirror can be evaluated separately. Figs. 5(*c*) and 5(*e*) show two-dimensional (2D) plots of divergence measurements on the horizontal axis *versus* position along the mirror on the vertical axis, while (*d*) and (*f*) show these measurements integrated over the mirror positions. Panels (*c*) and (*d*) refer to measurements in the vertical direction (MS1), while panels (*e*) and (*f*) refer to measurements in the horizontal direction (MS2). Considering Fig. 5(*c*), reflection maxima from the central region of the mirror (-40 mm $< x <$ 30 mm) are narrowly distributed around their average angle, while reflection angles from the region near the far end (30 mm $< x <$ 60 mm) deviate to higher values. For $x < -40$ mm, the reflection intensity is very low, with angles deviating to much lower values. From the integrated rocking curve shown in Fig. 5(*d*), the FWHM is ~39 μrad which, after deconvoluting the instrument resolution, implies that MS1 collimates the beam to ~18 μrad. Thus, the region between -40 mm and +60 mm can be considered to produce good collimation in the vertical direction.

Now switching to MS2, it is immediately apparent from Fig. 5(*e*) that reflection maxima are distributed over a larger angular range than in the case of MS1. Only in the region between -10 mm and +40 mm are angles narrowly distributed, while they deviate to higher angles in the region from +40 mm to +70 mm, and fluctuate widely for -50 mm to -10 mm. From the integrated rocking curve shown in Fig. 5(*f*), the FWHM is ~102 μrad which, after deconvolution, yields a divergence of 96 μrad. Judging from this, the MS2 region from -50 mm to +70 mm can be deemed usable, but produces considerably poorer collimation than MS1.

5. Ray-tracing simulations

Ray-tracing simulations of the actual measurement setup (*cf.* Fig. 2) were carried out, using the metrology measurement results together with mirror design parameters as inputs. For the working distance, the optimized value of 197 mm, as determined in the fine-alignment procedure, was used instead of the design value of 200 mm. Figs. 6(*a*) and 6(*b*) are simulations of the divergence measurements presented in Figs. 5(*c*) and 5(*e*). For both MS1 and MS2, the peak positions shift dramatically to lower angles for $x < -40$ mm, which results in a decreased reflectivity due to mismatches between local incident angles and Bragg angles. Given that measurements [*cf.* Fig. 5(*c*) and 5(*e*)] indicate almost no reflected intensity near the mirror ends, simulations shown in Figs. 6(*c*) and 6(*d*) are restricted to the regions considered to produce good collimation. With that restriction, the simulation results show

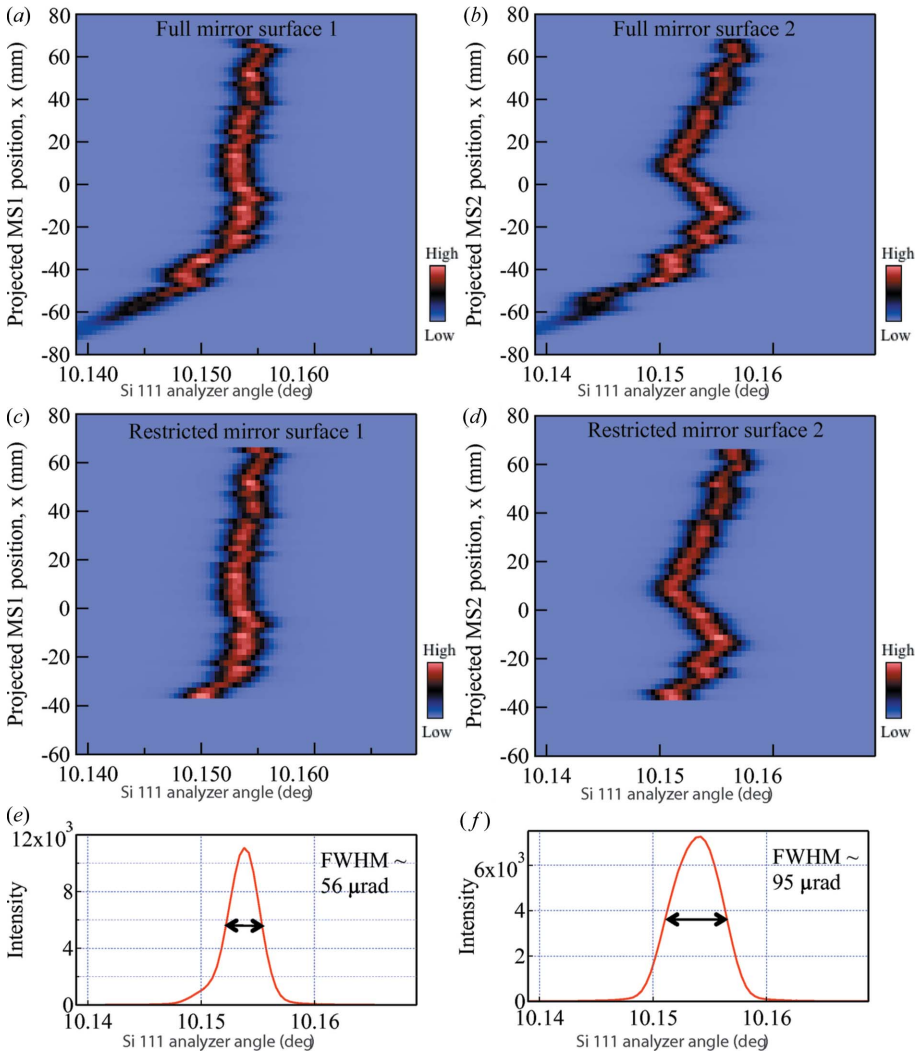

Figure 6
Ray-tracing simulation results. (*a*) and (*b*) 2D plots of divergence *versus* position along the mirror for MS1 and MS2, respectively. (*c*) and (*d*) Same divergence simulations now restricted to regions producing good collimation. (*e*) and (*f*) Integrated rocking curves of MS1 and MS2, respectively..

good agreement with the experimental results; the pattern of reflection maxima in the simulations matches the pattern in the measurements very well. These patterns directly correspond to the height error profiles [*cf.* Figs. 3(*a*) and 3(*b*)]; however, it should be noted that the optical measurements only sample a narrow strip, while the X-rays illuminate the whole mirror surface.

Figs. 6(*e*) and 6(*f*) show the simulated integrated rocking curves of the restricted profiles for MS1 and MS2, respectively. For MS1, the FWHM is 56 µrad, which is larger than the measured value of 39 µrad. This difference is probably due to the fact that outlying features near the mirror ends, which widen the integrated rocking curve, are less intense in the measurements than in the simulations. The integrated rocking curve of MS2, shown in Fig. 6(*f*), has a FWHM of 95 µrad, consistent with the measured value of 102 µrad.

Up to this point, all simulations were performed with a 5 µm-diameter scattering source, following the measurement setup. For an actual RIXS experiment, the scattering source size is larger, typically 10 µm × 40 µm (V × H). Consequently, simulations were repeated for such a source size. Beam divergences are shown in Fig. 7. The collimation performance is now dominated by the larger horizontal source size and leading to a larger horizontal beam divergence of 213 µrad FWHM. In the vertical direction, the beam divergence becomes 83 µrad FWHM. The shoulder peak in the vertical direction could be eliminated by adjusting the entrance aperture to block the near end of the mirror. Considering that the proposed multi-crystal analyzer system has an angular acceptance of ~100 µrad in its vertical diffraction plane, the degree of collimation by the Montel mirror in this direction is more than sufficient. In the horizontal direction, the angular acceptance of the analyzer is greatly relaxed, thus the larger divergence emerging from the mirror is not expected to significantly decrease throughput.

6. Discussion

As described above, the Montel mirror fulfils the basic requirements for use as the collimating element of a multi-crystal analyzer system for high-resolution RIXS measurements. However, further improvements of the collimation quality and angular acceptance are

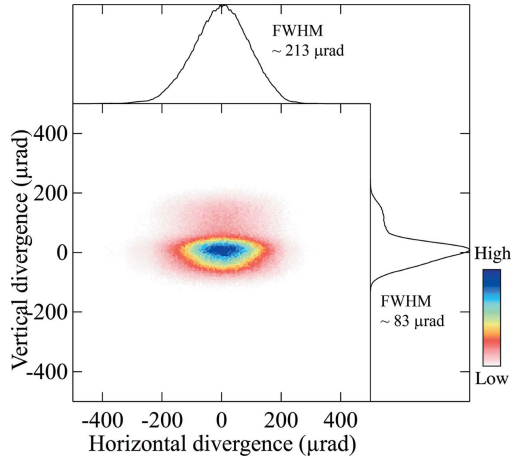

Figure 7
Simulated beam divergences using a typical scattering source size for RIXS measurements [10 µm × 40 µm (V × H)] and measured mirror surface profiles (*cf.* Fig. 3). The full unrestricted mirror lengths were used in this calculation.

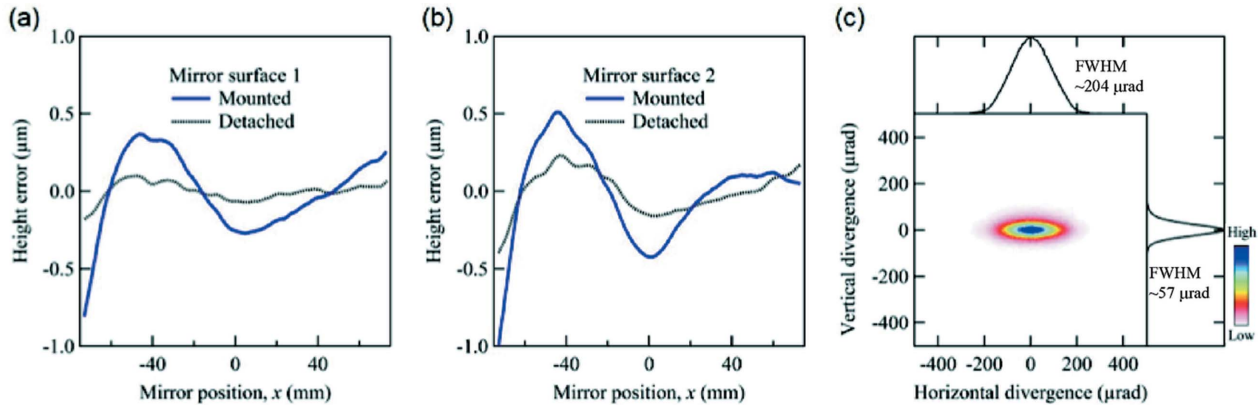

Figure 8
Height error profiles for (*a*) MS1 and (*b*) MS2. (*c*) Simulated beam divergence for the detached mirror case.

possible. Figure errors are the key factor that adversely affects the performance of the mirror. Reducing the figure errors and improving the quality of the multilayer would in turn increase collimation and enlarge the angular acceptance.

In addition to intrinsic figure errors, the figure of the mirror could be further degraded by mounting stresses. In order to explore the best achievable performance, the optical metrology measurements were repeated with the mirror detached from its mounting frame. Height error profiles for both mirror surfaces, mounted and detached, are presented in Figs. 8(*a*) and 8(*b*). Standard deviations of the height (slope) errors for the detached case are 55 nm (6.8 μrad) for MS1 and 130 nm (13 μrad) for MS2, smaller than those in the mounted case. Using these profiles, ray-tracing simulations [*cf.* Fig. 8(*c*)] were repeated and show a similar horizontal divergence of 204 μrad, still dominated by the horizontal scatter source size. But, for the vertical direction, the divergence is now 57 μrad, significantly smaller than in the mounted case. Furthermore, the shoulder peak is now absent, even when the full mirror length is included. Therefore, paying close attention to strain-free mounting can greatly improve the performance of the mirror.

7. Conclusions

A laterally graded, parabolic, multilayer Montel mirror was designed as collimating element of a multi-crystal analyzer system, intended for high-resolution RIXS measurements at the Ir L_3-absorption edge. In contrast to other studies, the collimation performance and angular acceptance of the device were directly measured at the 27-ID beamline of the APS. For a small 5 μm scattering source, both mirror surfaces collected scattered X-rays over a larger than required angular acceptance of 10 mrad and provided good collimation of less than 100 μrad. In the case of a larger source, as in a typical RIXS experiment, the collimation quality of the mirror was found to be somewhat degraded, but still suitable for use in a multi-crystal analyzer system. Ray-tracing simulations based on optical metrology measurements closely reproduced the observed X-ray collimation results. Improvements in mirror figure, multilayer quality and strain-free mounting of this device will further improve its performance.

Acknowledgements

The authors would like to thank M. G. Honnicke for the initial design of the Montel mirror. Use of the Advanced Photon Source, an Office of Science User Facility operated for the US DOE Office of Science by Argonne National Laboratory, was supported by the US DOE under Contract No. DE-AC02-06CH11357.

References

Ament, L. J. P., van Veenendaal, M., Devereaux, T. P., Hill, J. P. & van den Brink, J. (2011). *Rev. Mod. Phys.* **83**, 705–767.
Cai, Y., Coburn, D., Cunsolo, A., Keister, J., Honnicke, M., Huang, X., Kodituwakku, C., Stetsko, Y., Suvorov, A., Hiraoka, N., Tsuei, K. D. & Wille, H. C. (2013). *J. Phys. Conf. Ser.* **425**, 202001.
Gog, T., Casa, D. M., Said, A. H., Upton, M. H., Kim, J., Kuzmenko, I., Huang, X. & Khachatryan, R. (2013). *J. Synchrotron Rad.* **20**, 74–79.
Honnicke, M. G., Keister, J. W., Conley, R., Kaznatcheev, K., Takacs, P. Z., Coburn, D. S., Reffi, L. & Cai, Y. Q. (2011). *J. Synchrotron Rad.* **18**, 862–870.
Huang, X.-R. (2011). *J. Synchrotron Rad.* **18**, 899–906.
Jackeli, G. & Khaliullin, G. (2009). *Phys. Rev. Lett.* **102**, 017205.
Kao, C.-C., Caliebe, W., Hastings, J. & Gillet, J. (1996). *Phys. Rev. B*, **54**, 16361–16364.
Kim, B. J., Jin, H., Moon, S. J., Kim, J.-Y., Park, B.-G., Leem, C. S., Yu, J., Noh, T. W., Kim, C., Oh, S.-J., Park, J.-H., Durairaj, V., Cao, G. & Rotenberg, E. (2008). *Phys. Rev. Lett.* **101**, 076402.
Kim, B. J., Ohsumi, H., Komesu, T., Sakai, S., Morita, T., Takagi, H. & Arima, T. (2009). *Science*, **323**, 1329–1332.
Kim, J., Casa, D., Upton, M. H., Gog, T., Kim, Y.-J., Mitchell, J. F., van Veenendaal, M., Daghofer, M., van den Brink, J., Khaliullin, G. & Kim, B. J. (2012*a*). *Phys. Rev. Lett.* **108**, 177003.
Kim, J., Daghofer, M., Said, A. H., Gog, T., van den Brink, J., Khaliullin, G. & Kim, B. J. (2014). *Nat. Commun.* **5**, 5453.
Kim, J., Said, A. H., Casa, D., Upton, M. H., Gog, T., Daghofer, M., Jackeli, G., van den Brink, J., Khaliullin, G. & Kim, B. J. (2012*b*). *Phys. Rev. Lett.* **109**, 157402.
Mundboth, K., Sutter, J., Laundy, D., Collins, S., Stoupin, S. & Shvyd'ko, Y. (2014). *J. Synchrotron Rad.* **21**, 16–23.
Shvyd'ko, Y., Stoupin, S., Shu, D., Collins, S. P., Mundboth, K., Sutter, J. & Tolkiehn, M. (2014). *Nat. Commun.* **5**, 5219.
Suvorov, A., Coburn, D. S., Cunsolo, A., Keister, J. W., Upton, M. H. & Cai, Y. Q. (2014). *J. Synchrotron Rad.* **21**, 473–478.